Title: Paleoenvironmental change recorded in submarine fans: the Eocene-Oligocene climate transition in the Alpine foreland basin

Authors: Euan L. Soutter[1*], Ian A. Kane[1], Ander Martínez-Doñate[1], Adrian J. Boyce[2], Jack Stacey[1] and Sébastien Castelltort[3]

Institutions:

[1*]Department of Earth and Environmental Sciences, University of Manchester, Manchester, U.K.

[2]Scottish Universities Environmental Research Centre, East Kilbride, U.K.

[3]Department of Earth Sciences, University of Geneva, Geneva, Switzerland.

Email: euan.soutter@manchester.ac.uk

ABSTRACT

The Eocene-Oligocene transition (EOT) was a period of considerable environmental change, signifying the transition from Paleocene greenhouse to Oligocene icehouse conditions. Preservation of the sedimentary signal of such an environmental change is most likely in net-depositional environments, such as submarine fans, which are the terminal parts of sedimentary systems. Here, using sedimentological and stable isotope data from the Alpine foreland basin, we assess whether this major climatic transition influenced the stratigraphic evolution of submarine fans. Results indicate that submarine fan retreat in the Alpine foreland basin corresponds with positive $\delta^{13}C$ excursions related to major global perturbations of the carbon cycle and cooling in the earliest Oligocene. Submarine fan retreat is suggested to be influenced by this cooling through enhanced aridity and reduced subaerial runoff from the Corsica-Sardinia hinterland. The influence of aridity was periodically overwhelmed by local environmental factors, such as hinterland uplift, which increased sediment supply to deep-water during arid periods. These results highlight that: 1) hinterland climate may play a greater role than sea-level in dictating sediment supply to deep-water and, 2) submarine fan evolution occurs through a complex interplay between climate, eustasy and tectonics, which makes robust interpretations of paleoenvironmental change from their stratigraphic record, without multi-proxy records, difficult.

INTRODUCTION

The stratigraphic record of major environmental change is expected to be best recorded in net-depositional environments, such as submarine fans. Submarine fans are built from the deposits of sediment-gravity flows that transport vast quantities of terrigenous sediment and organic carbon to deep-marine environments (Curray and Moore, 1971; Leithold et al., 2016). Submarine fan growth has been shown to occur during both low and high eustatic sea levels (e.g. Covault et al. 2007) and may be driven by a combination of tectonic (e.g. Howarth et al. 2021) and climatic processes (e.g. Picot et al. 2019), all of which may be overprinted by autogenic processes. Disentangling allogenic from autogenic influences on submarine fan deposition has therefore proven to be difficult (e.g. Ferguson et al. 2020). Measurement of $\delta^{13}C$ in carbonates, foraminifera and organic carbon, has been used as a means of addressing this problem, with $\delta^{13}C$ sensitive to many of the environmental changes expected to influence submarine fan deposition (e.g. Castelletort et al. 2017).

The Eocene-Oligocene climate transition (EOT) between ~34 and ~33 Ma was a major environmental response to the opening of oceanic gateways in the Southern Oceans (Kennett, 1977), decreased atmospheric CO_2 (Pearson et al. 2009) and orbital forcing (Ladant et al. 2014). Effects of this environmental response include the establishment of major Antarctic ice sheets (Liu et al. 2009) and the transition from Paleogene greenhouse to current icehouse conditions (Wade et al. 2012). The EOT occurred through a series of global cooling 'steps' that correspond to positive $\delta^{18}O$ and $\delta^{13}C$ excursions (Katz et al. 2008; Armstrong McKay et al. 2016), such as the 'Oi-1' event at ~33.55 ma, which is interpreted to represent a major eustatic sea-level fall related to Antarctic ice sheet growth (Katz et al. 2008).

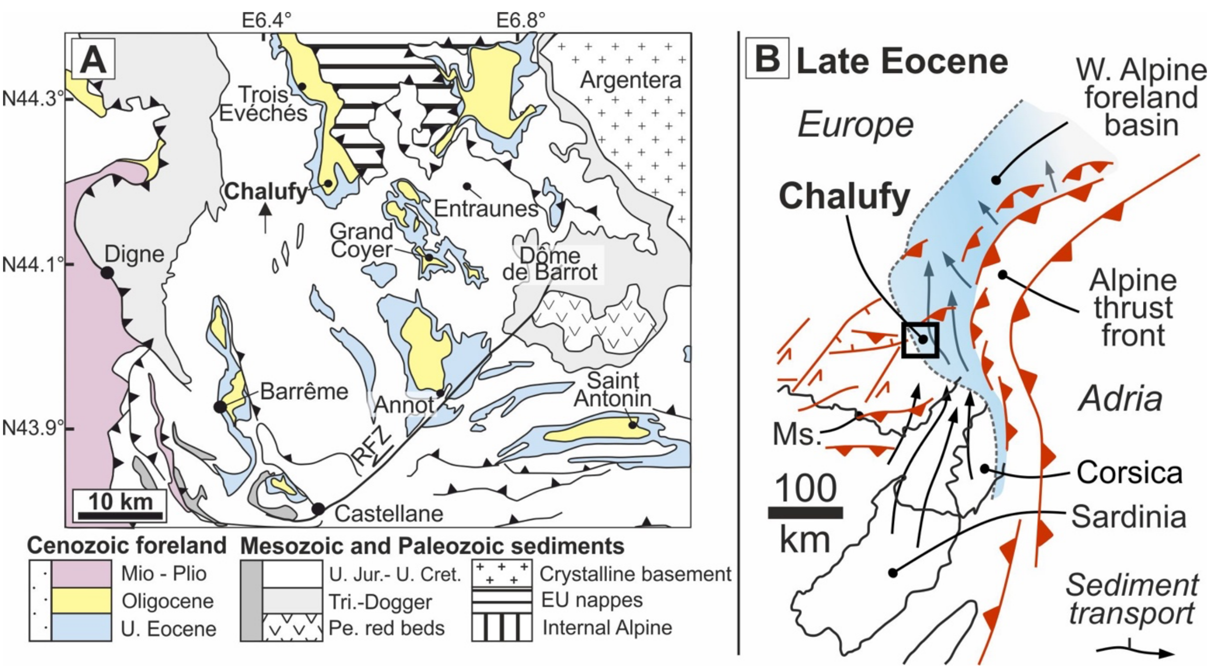

The Grès d'Annot Formation is an exhumed siliciclastic deep-marine succession that was deposited within the Alpine foreland basin (Fig. 1A and 1B) during the EOT (Fig. 2A) (Joseph and Lomas, 2004). The Grès d'Annot records a common deep-marine stratigraphic pattern of fine-grained intervals interspersed with coarser-grained intervals. This cyclicity has been attributed to sea-level changes and tectonism (Fig. 1B) (Callec, 2004, Euzen et al. 2004); however, the relative impact of these controls has not been tested. This study, therefore, aims to investigate, through high-resolution isotopic analysis of the Grès d'Annot stratigraphy, whether submarine fan growth in the Alpine foreland basin was related to the Eocene – Oligocene transition and associated climatic upheaval. On a broader scale, this study aims to explore how the isotopic records of exhumed submarine fans can be used to understand how past landscapes responded to environmental change.

STUDY AREA: CHALUFY

One of the most well-studied Grès d'Annot exposures is located at the Montagne de Chalufy (Fig. 1A; B), representing a relatively distal part of the Grès d'Annot submarine fan system (Fig. 1A; Fig. S1). The exposure comprises three prominent coarse-grained sandstone intervals deposited sequentially against a marl paleo-slope (Puigdefabregas et al. 2004) (Fig. 2B). The coarse-grained intervals are interpreted as the deposits of high-concentration turbidity currents that built submarine fan lobes on the basin floor. These coarse-grained intervals alternate with finer-grained mudstone and siltstone intervals, which are interpreted as the deposits of lower-concentration turbidity currents, interbedded with thin hemipelagic mudstones deposited at the distal extents of the coarse-grained lobes or distributary channels on the basin floor (Fig. 2B; Supplementary Fig. 2). One of these coarse-grained intervals (Sandstone 3) can be correlated northwards from within the uppermost fine-grained interval, where it overlies an erosion surface incising the underlying coarse-grained interval (Joseph et al. 2000) (Fig. 2B).

Identification of foraminifera belonging to known planktonic (P) and nano-planktonic (NP) biozones indicates that the basal part of the Grès d'Annot exposed at Chalufy was deposited at a maximum of 34.2 Ma (NP20/NP21), with the uppermost parts of the Grès d'Annot being deposited at a maximum of 32.8 Ma (NP21/22) or 32 Ma (top P18) (Fig. 2A) (Euzen et al. 2004; Du Fornel et al. 2004). The base of P18 occurs prior to the first coarse-grained interval (Fig. 2A) (Du Fornel et al. 2004). For consistency with the existing Alpine foreland chronostratigraphic framework, and the other isotopic and eustatic datasets used (Cramer er al. 2009; Miller et al. 2008), all ages are tied to Berggren et als. (1995) chronology.

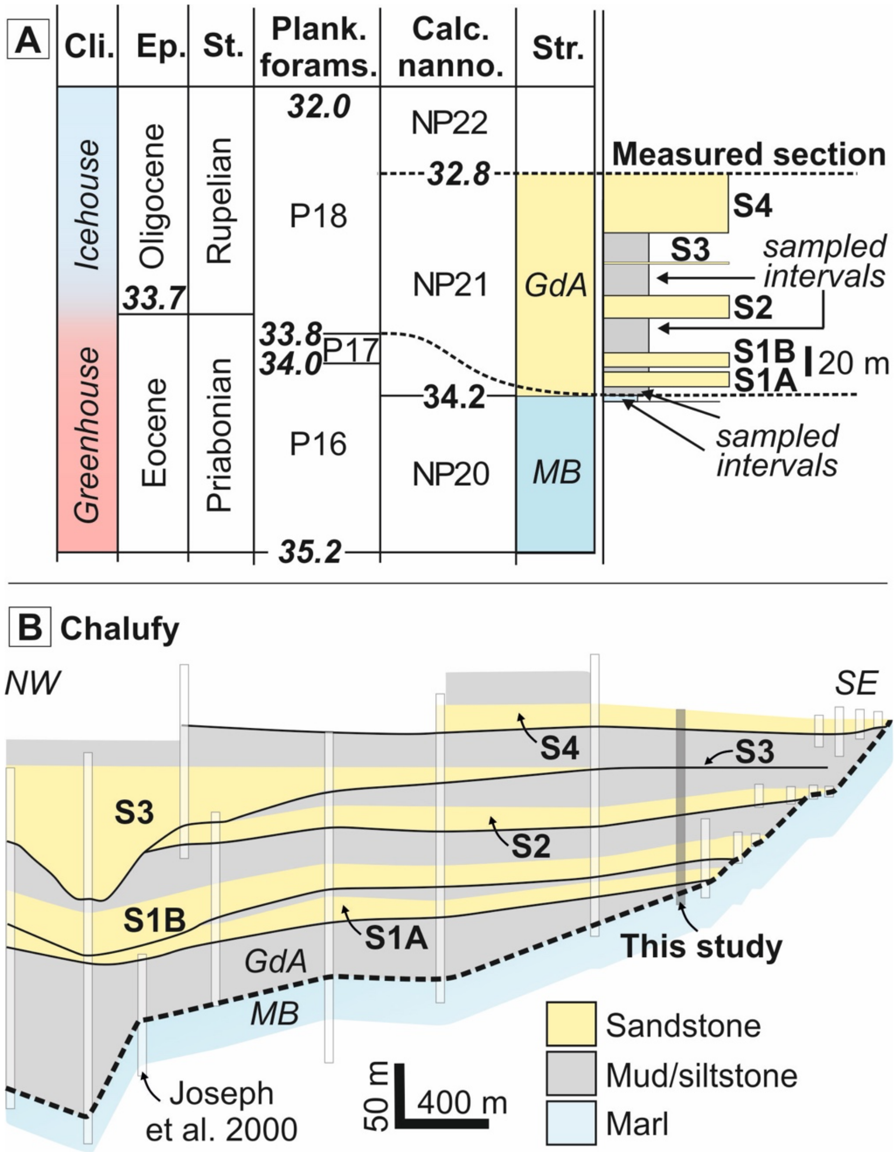

DATA AND METHODS

111 samples were recovered from three fine-grained intervals in one continuous measured section spanning the Grès d'Annot exposure at the Chalufy paleo-slope (Fig. 3; Fig. S1, S2; S3; Table S1). The samples were collected at ~50 cm intervals, from > 30 cm below the exposed surface and only within hemipelagic sections, thus avoiding potential contamination by allochthonous material. The samples were crushed and their bulk carbonate $\delta^{13}C$ and $\delta^{18}O$ values measured using standard techniques (Brodie et al. 2018), with 9 repeated measurements of section representative samples yielding a mean measurement error of ± 0.3 for $\delta^{13}C$ and ± 0.1 for $\delta^{18}O$ (Fig. 2; S3). Carbon and oxygen isotopes are reported per mil (‰) relative to the Vienna Pee Dee Belemnite Standard (VPDB) (Fig. S3).

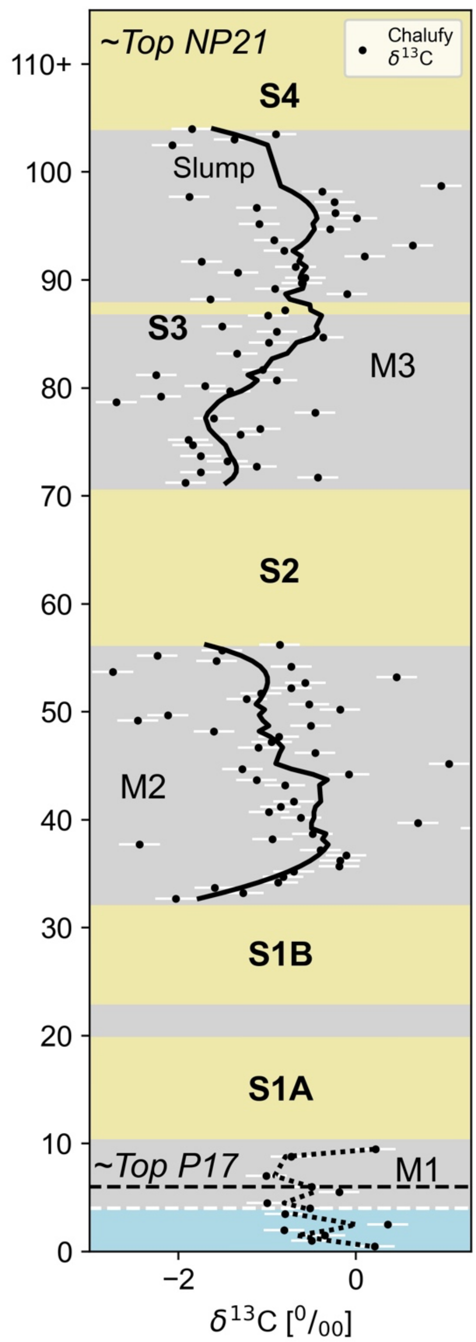

Three isotopic curves representing each fine-grained interval were generated through the application of a Savitzky–Golay filter to the individual data points, which smooths the data without distorting the underlying signal (Fig. 3; S3; S4; S8) (Savitzky and Golay, 1964). These curves were then placed within bounding-age constraints derived from micropaleontological zonation of the study area (Du Fornel et al. 2004) and assessed for correlation with time-equivalent data compilations; the global $\delta^{13}C$ curve (Cramer et al. 2009) and the North Atlantic eustatic sea-level curve (Miller et al. 2005). Randomly selected samples from the fine-grained sections have also undergone X-ray diffraction (XRD), total organic carbon (TOC) (Table S1) and petrographic analysis (Fig. S7) in order to assess the potential for mixed-carbonate-source error or diagenetic overprinting.

RESULTS

The bulk $\delta^{13}C_{VPDB}$ content was measured from 111 samples (Fig. 3; Fig. S2). The identification of benthic foraminifera in the petrographic analysis of the samples (Fig. S7) and the occurrence of dateable benthic foraminifera within the Chalufy section (Fig. 2A) indicates that the bulk $\delta^{13}C$ measurements primarily record the signature of this fauna. The observed depletion in $\delta^{18}O$ values suggests some diagenetic influence, which may have also impacted the $\delta^{13}C$ values. Cross-plotting of $\delta^{13}C$ and $\delta^{18}O$ from each interval also shows no statistically-significant trends, however, suggesting a lack of diagenetic overprinting (Marshall, 1991) (Fig. S6). X-ray diffraction of selected samples within each interval indicates total organic carbon (TOC) contents of < 0.7 % and calcite to organic matter ratio of > 7:1, reducing the likelihood of diagenetic contamination from organic carbon (Saltzmann and Thomas, 2012).

The $\delta^{13}C$ data shows a broadly increasing spread with increasing height in the section (1σ = 0.5 ‰, 0.4 ‰, 0.9 ‰, 1.0 ‰ for each sequential fine-grained interval) (Fig. S5), with mean $\delta^{13}C$ values being 2.0 ‰ more negative than time-equivalent open oceanic values. (Cramer et al., 2009). Data noise, more negative $\delta^{13}C$ values, and signal amplification are attributed to 1) microscopic turbidites or authigenic carbonate, such as micro-veins, within the hemipelagic sections creating allochthonous noise (Fig. S7); and 2) the relatively proximal position of the basin resulting in the oxidation of light organic ^{12}C delivered by rivers (Jenkyns, 1996; Voigt and Hilbrecht, 1997). These unavoidable diagenetic and environmental factors potentially acted to adjust the isotopic values. However, this is mitigated by the high sampling density, which allows the underlying, primary isotopic trends to be resolved.

The Chalufy $\delta^{13}C$ curves of Mudstone 2 (M2) and Mudstone 3 (M3) (sandstone-bounded fine-grained intervals) each show a general trend of increasing then decreasing $\delta^{13}C$ values with height (Fig. 3), and show good correlation with the oceanic $\delta^{13}C$ curve, with two positive global $\delta^{13}C$ excursions seen across the EOT in the early Oligocene observed within these data (Fig. 4). The Chalufy $\delta^{18}O$ values show a generally decreasing, but noisy, trend in M2, and a sharply increasing then sharply decreasing trend in M3. However, due to diagenesis, these δ18O trends are expected to be less reliable than the $\delta^{13}C$ trends (Fig. S3).

Sandstone 3 (S3) is thin-bedded and fine-grained in the measured section, but thickens northwards due to channelization (Fig. 2B), where it correlates with a sustained period of positive $\delta^{13}C$ values (Fig. 3) and a sharp positive $\delta^{18}O$ excursion (Fig. S3). The exact depositional duration of this channel is uncertain due to this interval representing a sustained period of bypass and erosion. However, deposition within the channel must have ceased by mid-way through M3, as the upper half of M3 overlies the channel-fill (Fig. 2B).

There is uncertainty in how much time is occupied between the upper marl surface and Grès d'Annot deposition as the older part of the stratigraphy is not present in this location on the basin margin slope but is preserved within deeper parts of the basin (Fig. 2B). Accordingly, the isotopic trends within the lowermost sections cannot be confidently interpreted.

DISCUSSION

The observed correlation between submarine fan retreat and global positive $\delta^{13}C$ excursions indicates that deposition in the Alpine foreland was influenced by global environmental change across the EOT, with positive $\delta^{13}C$ excursions during this period attributed to; 1) low sea-levels, increased weathering of $\delta^{13}C$-enriched carbonate shelves and deepening of the CCD, 2) increased ocean mixing and productivity, and 3) cooling and sequestration of ^{12}C in permafrost (Armstrong McKay et al. 2016). These factors are related to cooling. Therefore, if the $\delta^{13}C$ record of the Alpine foreland represents the global signature, this indicates that periods of reduced deep-water sedimentation in the Alpine foreland were driven by global cooling across the EOT.

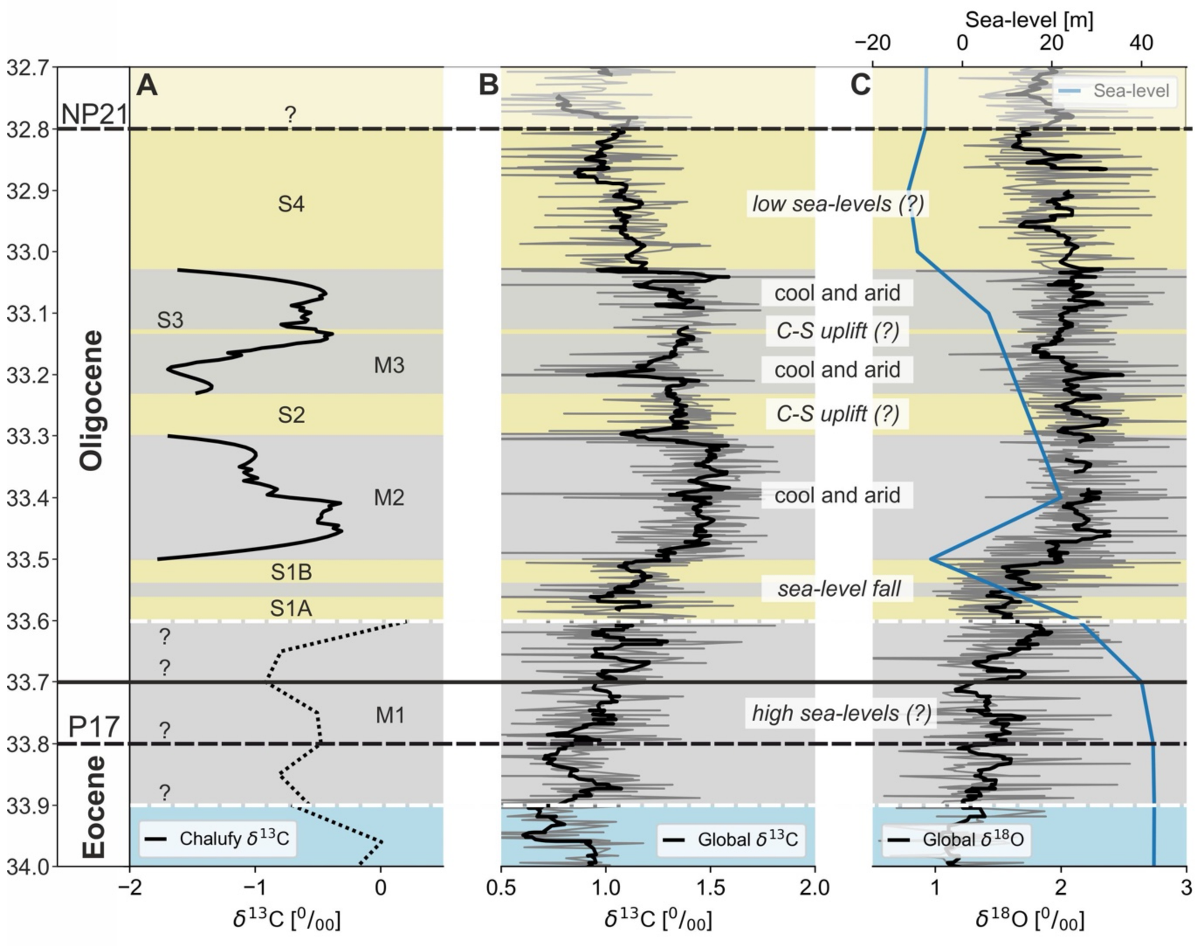

Cooler climates may reduce sediment supply by enhancing aridity and reducing runoff (e.g. Leeder et al. 1998), perhaps indicating that the Corsica-Sardinia source area was influenced by early Oligocene climate change (Fig. 1). This effect may also be reflected in the $\delta^{13}C$ record of the fine-grained sections, with a reduction in the volume of ^{12}C transported to marine environments by rivers consistent with the observed positive $\delta^{13}C$ excursions (Voigt and Hilbrecht, 1997). Similar depositional patterns have been observed during the Quaternary, with aridity associated with submarine fan retreat in both the Congo (Picot et al. 2019) and Nile (Ducassou et al. 2009) submarine fans irrespective of sea-level. These findings indicate a similar climatic control on deep-water deposition in the Alpine foreland.

This results in a contrast, with periods of coarse-grained sedimentation also observed to occur during sustained positive $\delta^{13}C$ excursions, and therefore cooler temperatures and aridity. This is suggested to have resulted from periods of concurrent tectonism and uplift in the Corsica-Sardinian hinterland (Advokaat et al. 2014), which will have temporarily overwhelmed the influence of aridity, causing submarine fan advance. It's also possible that cooling and the sharp $\delta^{18}O$ excursion correlated with S3 represents the point at which sea-level was lowered enough to overwhelm the influence of onshore aridity (Fig. S3), which may be related to the Oi-1a excursion and associated sea-level fall identified elsewhere (Katz et al. 2008).

When compared to the eustatic trend, it is tempting to correlate early sandstone deposition (S1A and S1B) to the negative $\delta^{18}O$ excursion and major sea-level fall seen at the Eocene-Oligocene boundary, however the lack of basal age constraint makes this uncertain (Fig. 4). There is more confidence in interpreting the rising sea-level at 33.5 Ma as related to fine-grained deposition (M2) and the lowstand at 33 Ma as being related to coarse-grained deposition (S4), which would indicate eustasy influenced sediment delivery to deep-water. The positive $\delta^{13}C$ excursions within the fine-grained intervals may therefore represent sea-level highstands (e.g. Castelltort et al. 2017). However, this would imply warming during the positive $\delta^{13}C$ excursions, which is counter to the prevailing interpretation that the global $\delta^{13}C$ excursions during this period are related to periods of enhanced cooling (Armstrong McKay et al. 2016). This might suggest that onshore climate was more influential than eustasy, or that relative sea-level change unresolved by eustatic trends influenced deep-marine sedimentation.

CONCLUSION

Submarine fan evolution is intimately linked to tectonic and climatic processes. The stratigraphic record of submarine fans is therefore expected to archive major tectonic and climatic events. Here we show that positive $\delta^{13}C$ excursions associated with major global carbon cycle perturbations correspond to periods of reduced sediment delivery to the Alpine foreland basin. This is likely to be caused by global cooling and enhanced aridity, which reduced runoff and decreased sediment supply to deep-marine environments. The influence of aridity was periodically overwhelmed by uplift in the tectonically-active hinterland, resulting in increased sediment supply to deep-water. This study indicates that onshore climate can be more influential than sea-level change in controlling deep-water deposition, further highlighting the complex interplay of climatic and tectonic processes in influencing sediment supply to deep-water environments.

ACKNOWLEDGEMENTS

Soutter is funded by Natural Environment Research Council grant number NE/M00578X/1. We wish to thank Julie Dougans (SUERC) for technical assistance in the stable isotope analyses.

FIGURE CAPTIONS

Figure 1: A) Geological map of the Alpine foreland and the location of the sampled section at Montagne de Chalufy (black arrow). Lines with black ticks represent thrust faults. (modified from Joseph and Lomas, 2004). U. = upper; Mio-Plio = Miocene-Pliocene; Jur. = Jurassic; Cret. = Cretaceous, Tri. = Triassic; Pe = Permian. EU = Embrunais-Ubaye. B) Palinspastic reconstruction and paleogeographic setting of the Alpine foreland basin during the Late Eocene (modified from Dumont et al. 2011). Ms = Marseille.

Figure 2: A) Chronostratigraphic framework of the studied section (modified from Euzen et al., 2004). The base of P18 is expected to be intersected before S1A. B) Correlation of the Chalufy outcrop and sampled section, with sandstone labels indicated (modified from Joseph et al. (2000). Micropaleontological zonation of the studied stratigraphy (modified from Euzen et al. 2004). Eocene – Oligocene boundary shifted to that of Katz et al. (2008). GdA = Gres d'Annot; MB = Marnes Bleues; Cli. = generalized climate; Ep. = epoch; St. = stage, Plank. forams = planktonic foraminifera; Calc. nano. = calcareous nannofossils; Strat: stratigraphy.

Figure 3: δ^{13}C measurements for each fine-grained interval sampled and their bounding P Zones (Du Fornel et al. 2004). The black solid line represents a Savitzky-Golay filter. Yellow = sandstone, grey = mudstone and siltstone, blue = marl. The white line is an uncertain age break, and the solid yellow line

correlates with the top of the channelized sand 3 preserved to the north (Fig. 1B). Error bar is the mean error of $\delta^{13}C$ standards.

Figure 4: Correlation between A) the $\delta^{13}C$ record of Chalufy, B) Global $\delta^{13}C$ curve (Cramer et al. 2008), and C) Global $\delta^{18}O$ curve and North Atlantic sea-level (Miller et al. 2005). C-S = Corsica-Sardinia, yellow = sandstone, grey = mudstone and siltstone, blue = marl. Ages tied to the chronology of (Bergrenn et al. 1995; Cande and Kent, 1995). The white line indicates uncertain age break. Solid black lines are Savitzky–Golay filtered data, grey lines indicate raw data.

SUPPLEMENTARY CAPTIONS

Table S1: All of the geochemical data collected for this manuscript and associated stratigraphic height.

Figure S1: Measured and sampled sections at Chalufy and stratigraphic context. Red dashed line indicates a fault. Grid reference: 44°09’21”N, 6°32’51E.

Figure S2: Logged section at Chalufy and sample locations. Middle and upper sandstones from Puigdefabregas et al. (2004). Numbers refer to sand unit described in text.

Figure S3: $\delta^{13}C$ and $\delta^{18}O$ measurements for each fine-grained interval sampled and their bounding P Zones (Du Fornel et al. 2004). Yellow = sandstone, grey = mudstone and siltstone, blue = marl. The white line is an uncertain age break, and the solid yellow line correlates with the top of the channelized sand 3 preserved to the north (Fig. 1B). Error bar is the mean error of $\delta^{13}C$ and $\delta^{18}O$ standards.

Figure S4: Correlation between A) the $\delta^{13}C$ record of Chalufy, B) Global $\delta^{13}C$ curve (Cramer et al. 2008), C) the $\delta^{18}O$ record of Chalufy, and D) Global $\delta^{18}O$ curve and North Atlantic sea-level (Miller et al. 2005). C-S = Corsica-Sardinia, yellow = sandstone, grey = mudstone and siltstone, blue = marl. Ages tied to the chronology of (Bergrenn et al. 1995; Cande and Kent, 1995). The white line indicates uncertain age break. Solid black lines are Savitzky–Golay filtered data, grey lines indicate raw data.

Figure S5: Standard deviations of $\delta^{13}C$ and $\delta^{18}O$ data. Box indicates quartiles, black line indicates median, whiskers indicate the remainder of the distribution, diamonds indicate outliers determined through a method that is a function of the inter-quartile range.

Figure S6: Cross-plot of $\delta^{18}O$ v $\delta^{13}C$ indicates no correlation and therefore a minimum of diagenetic alteration. Rho (ρ) is spearman rank correlation, p is probability value (p-value)

Figure S7: Thin-section photomicrographs of samples: plane polarized light (PPL) (left) and cathodoluminescence (CL) (right). (A&B) Heterogeneous matrix comprised of mud (light brown in PPL) with silt sized detrital quartz and calcite grains (blue and orange luminescence respectively) and foraminifera (arrowed). Stable isotope measurements were derived from this foraminifera-rich material. (B&C) Minor fracture (white arrow) crosscut by a major fracture (red arrow) both cemented by dull blue luminescing calcite. The major fracture is approximately bed parallel, suggesting stylolite cementation. (D&E) Organic matter (dark brown to black in PPL) is bed parallel. Well-developed laminations of quartz-rich (red arrows) and calcite-rich (white arrows) sediment (blue and orange luminescence respectively). Scale bar is 500 μm.

Figure S8: Savitsky-Golay filters of different window lengths for the collected isotopic data.

REFERENCES

Advokaat, E.L., van Hinsbergen, D.J., Maffione, M., Langereis, C.G., Vissers, R.L., Cherchi, A., Schroeder, R., Madani, H. and Columbu, S., 2014, Eocene rotation of Sardinia, and the paleogeography of the western Mediterranean region: Earth and Planetary Science Letters, v. 401, p. 183-195.

Apps, G., Peel, F. and Elliott, T., 2004, The structural setting and palaeogeographical evolution of the Grès d'Annot basin: Geological Society, London, Special Publications, v. 221, p. 65-96.

Armstrong McKay, D.I., Tyrrell, T. and Wilson, P.A., 2016. Global carbon cycle perturbation across the Eocene-Oligocene climate transition. *Paleoceanography*, *31*(2), pp.311-329.

Berggren, W. A., Kent, D. V., Swisher, C. C. & Aubry, M.-P, 1995, Geochronology, Time Scales and Global Stratigraphic Correlations: A Unified Temporal Framework for an Historical Geology, eds Berggren, W. A., Kent, D. V. & Hardenbol, J.: SEPM, p. 129–212.

Brodie, M.W., Aplin, A.C., Hart, B., Orland, I.J., Valley, J.W. and Boyce, A.J., 2018, Oxygen isotope microanalysis by secondary ion mass spectrometry suggests continuous 300-million-year history of calcite cementation and dolomitization in the Devonian Bakken Formation: Journal of Sedimentary Research, v. 88, 91-104.

Cande, S.C. and Kent, D.V., 1995, Revised calibration of the geomagnetic polarity timescale for the Late Cretaceous and Cenozoic: Journal of Geophysical Research: Solid Earth, v. 100, p. 6093-6095.

Castelltort, S., Honegger, L., Adatte, T., Clark, J.D., Puigdefàbregas, C., Spangenberg, J.E., Dykstra, M.L. and Fildani, A., 2017, Detecting eustatic and tectonic signals with carbon isotopes in deep-marine strata, Eocene Ainsa Basin, Spanish Pyrenees: Geology, v. 45, p. 707-710.

Covault, J.A., Normark, W.R., Romans, B.W. and Graham, S.A., 2007, Highstand fans in the California borderland: The overlooked deep-water depositional systems: Geology, v. 35, p. 783-786.

Cramer, B.S., Toggweiler, J.R., Wright, J.D., Katz, M.E. and Miller, K.G., 2009. Ocean overturning since the Late Cretaceous: Inferences from a new benthic foraminiferal isotope compilation: Paleoceanography, v. 24.

Curray, J.R. and Moore, D.G., 1971, Growth of the Bengal deep-sea fan and denudation in the Himalayas: Geological Society of America Bulletin, v. 82, p. 563-572.

Du Fornel, E., Joseph, P., Desaubliaux, G., Eschard, R., Guillocheau, F., Lerat, O., Muller, C., Ravenne, C. and Sztrakos, K., 2004, The southern Grès d'Annot outcrops (French Alps): an attempt at regional correlation: Geological Society, London, Special Publications, v. 221, p. 137-160.

Ducassou, E., Migeon, S., Mulder, T., Murat, A., Capotondi, L., Bernasconi, S.M. and Mascle, J., 2009. Evolution of the Nile deep-sea turbidite system during the Late Quaternary: influence of climate change on fan sedimentation: Sedimentology, v. 56, p. 2061-2090.

Dumont, T., Simon-Labric, T., Authemayou, C. and Heymes, T., 2011. Lateral termination of the north-directed Alpine orogeny and onset of westward escape in the Western Alpine arc: Structural and sedimentary evidence from the external zone: Tectonics, v. 30.

Euzen, T., Joseph, P., Du Fornel, E., Lesur, S., Granjeon, D. and Guillocheau, F., 2004. Three-dimensional stratigraphic modelling of the Grès d'Annot system, Eocene-Oligocene, SE France. Geological Society, London, Special Publications, v. 221, p. 161-180.

Ferguson, R., Kane, I.A., Eggenhuisen, J., Pohl, F., Tilston, M., Spychala, Y. and Brunt, R., 2020, Entangled external and internal controls on submarine fan evolution: an experimental perspective: The Depositional Record.

Howarth, J.D., Orpin, A.R., Kaneko, Y. et al. 2021. Calibrating the marine turbidite palaeoseismometer using the 2016 Kaikōura earthquake: Nature Geoscience. In press.

Jenkyns, H.C., 1996, Relative sea-level change and carbon isotopes: Data from the upper Jurassic (Oxfordian) of central and Southern Europe: Terra Nova, v. 8, p. 75-85.

Joseph, P. and Lomas, S.A., 2004, Deep-water sedimentation in the Alpine Foreland Basin of SE France: New perspectives on the Grès d'Annot and related systems—an introduction: Geological Society, London, Special Publications, v. 221, p. 1-16.

Joseph, P., Babonneau, N., Bourgeois, A., Cotteret, G., Eschard, R., Garin, B., Gomes De Souza, O., Granjeon, D., Guillocheau, F., Lerat, O. and Quemener, J.M., 2000, December. The Annot Sandstone outcrops (French Alps): architecture description as input for quantification and 3D reservoir modeling. *in* P. Weimer, RM Slatt, J. Coleman, NC Rosen, H. Nelson, AH Bouma, MJ Styzen, and DT Lawrence, Deep-Water Reservoirs of the World: Gulf Coast Section SEPM Foundation 20th Annual Research Conference, SEPM CD Special Publication, v. 28, p. 422-449.

Katz, M.E., Miller, K.G., Wright, J.D., Wade, B.S., Browning, J.V., Cramer, B.S. and Rosenthal, Y., 2008, Stepwise transition from the Eocene greenhouse to the Oligocene icehouse: Nature Geoscience, v. 1, p. 329.

Kennett, J.P., 1977, Cenozoic evolution of Antarctic glaciation, the circum-Antarctic Ocean, and their impact on global paleoceanography: Journal of Geophysical Research, v. 82, p. 3843-3860.

Ladant, J.B., Donnadieu, Y., Lefebvre, V. and Dumas, C., 2014, The respective role of atmospheric carbon dioxide and orbital parameters on ice sheet evolution at the Eocene-Oligocene transition: Paleoceanography, v. 29, p. 810-823.

Leeder, M.R., Harris, T. and Kirkby, M.J., 1998. Sediment supply and climate change: implications for basin stratigraphy: Basin Research, v. 10, p. 7-18.

Leithold, E.L., Blair, N.E. and Wegmann, K.W., 2016. Source-to-sink sedimentary systems and global carbon burial: A river runs through it. Earth-Science Reviews, v. 153, p. 30-42.

Liu, Z., Pagani, M., Zinniker, D., DeConto, R., Huber, M., Brinkhuis, H., Shah, S.R., Leckie, R.M. and Pearson, A., 2009, Global cooling during the Eocene-Oligocene climate transition: Science, v. 323, p. 1187-1190.

Marshall, J.D., 1991, Climatic and oceanographic isotopic signals from the carbonate rock record and their preservation: Geological magazine, v. 129, p. 143-160.

Miller, K.G., Kominz, M.A., Browning, J.V., Wright, J.D., Mountain, G.S., Katz, M.E., Sugarman, P.J., Cramer, B.S., Christie-Blick, N. and Pekar, S.F., 2005, The Phanerozoic record of global sea-level change: Science, v. 310, p. 1293-1298.

Pearson, P.N., Foster, G.L. and Wade, B.S., 2009, Atmospheric carbon dioxide through the Eocene–Oligocene climate transition: Nature, v. 461, p. 1110.

Picot, M., Marsset, T., Droz, L., Dennielou, B., Baudin, F., Hermoso, M., De Rafélis, M., Sionneau, T., Cremer, M., Laurent, D. and Bez, M., 2019, Monsoon control on channel avulsions in the Late Quaternary Congo Fan: Quaternary Science Reviews, v. 204, p. 149-171.

Puigdefàbregas, C., Gjelberg, J. and Vaksdal, M., 2004, The Grès d'Annot in the Annot syncline: outer basin-margin onlap and associated soft-sediment deformation: Geological Society, London, Special Publications, v. 221, p. 367-388.

Saltzman, M.R., and Thomas, E., 2012, Carbon isotope stratigraphy, *in* Gradstein, F., et al., eds., The geologic time scale: Oxford, UK, Elsevier, p. 207–232.

Savitzky and M. J. E. Golay, 1964, Soothing and differentiation of data by simplified least squares procedures: *Anal. Chem.*, v. 36, p. 1627-1639.

Voigt, S. and Hilbrecht, H., 1997, Late Cretaceous carbon isotope stratigraphy in Europe: correlation and relations with sea level and sediment stability: Palaeogeography, Palaeoclimatology, Palaeoecology, v. 134, p. 39-59.

Weber, M.E., Wiedicke-Hombach, M., Kudrass, H.R. and Erlenkeuser, H., 2003, Bengal Fan sediment transport activity and response to climate forcing inferred from sediment physical properties: Sedimentary Geology, v. 155, p. 361-381.

Zachos, J.C. and Kump, L.R., 2005, Carbon cycle feedbacks and the initiation of Antarctic glaciation in the earliest Oligocene: Global and Planetary Change, v. 47, p. 51-66.

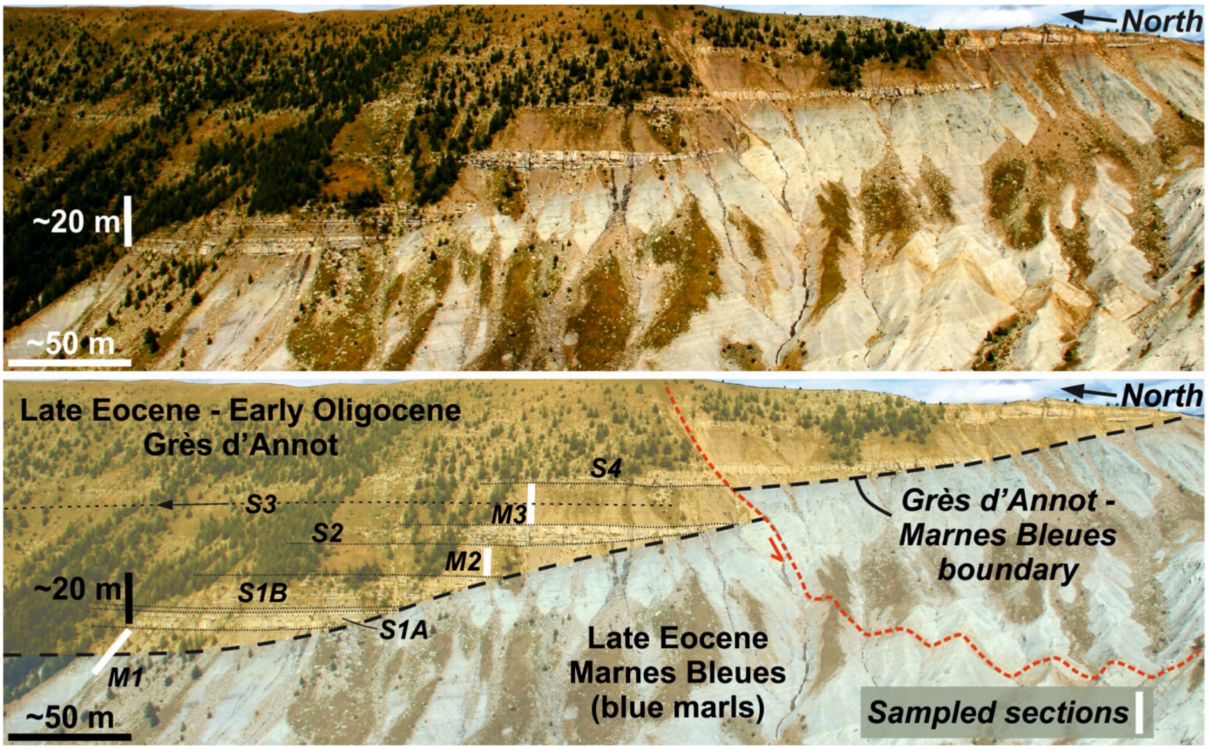
North
~20 m
~50 m
North
Late Eocene - Early Oligocene
Grès d'Annot
S4
S3
S2
M3
M2
S1B
S1A
~20 m
M1
~50 m
Grès d'Annot -
Marnes Bleues
boundary
Late Eocene
Marnes Bleues
(blue marls)
Sampled sections

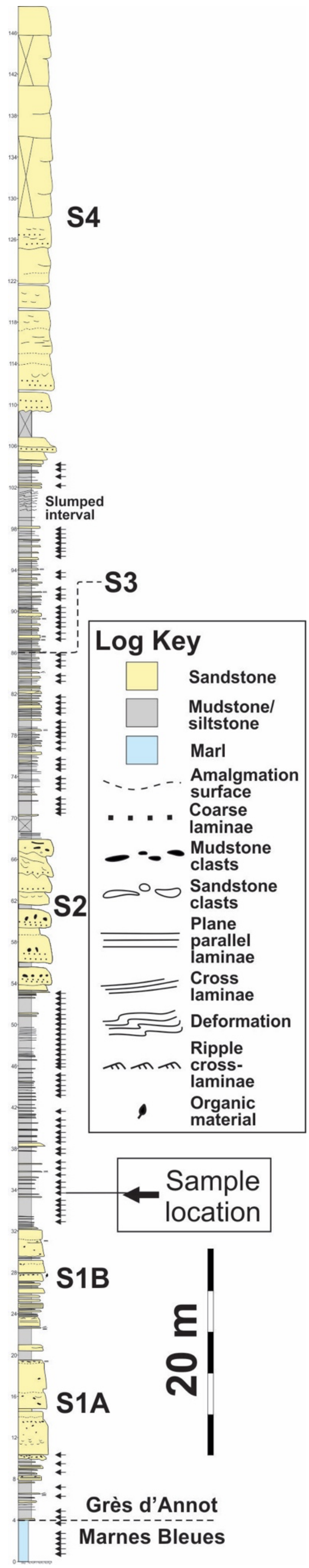
S4
Slumped interval
S3
Log Key
Sandstone
Mudstone/ siltstone
Marl
Amalgmation surface
Coarse laminae
Mudstone clasts
Sandstone clasts
Plane parallel laminae
Cross laminae
Deformation
Ripple cross-laminae
Organic material
S2
Sample location
S1B
20 m
S1A
Grès d'Annot
Marnes Bleues

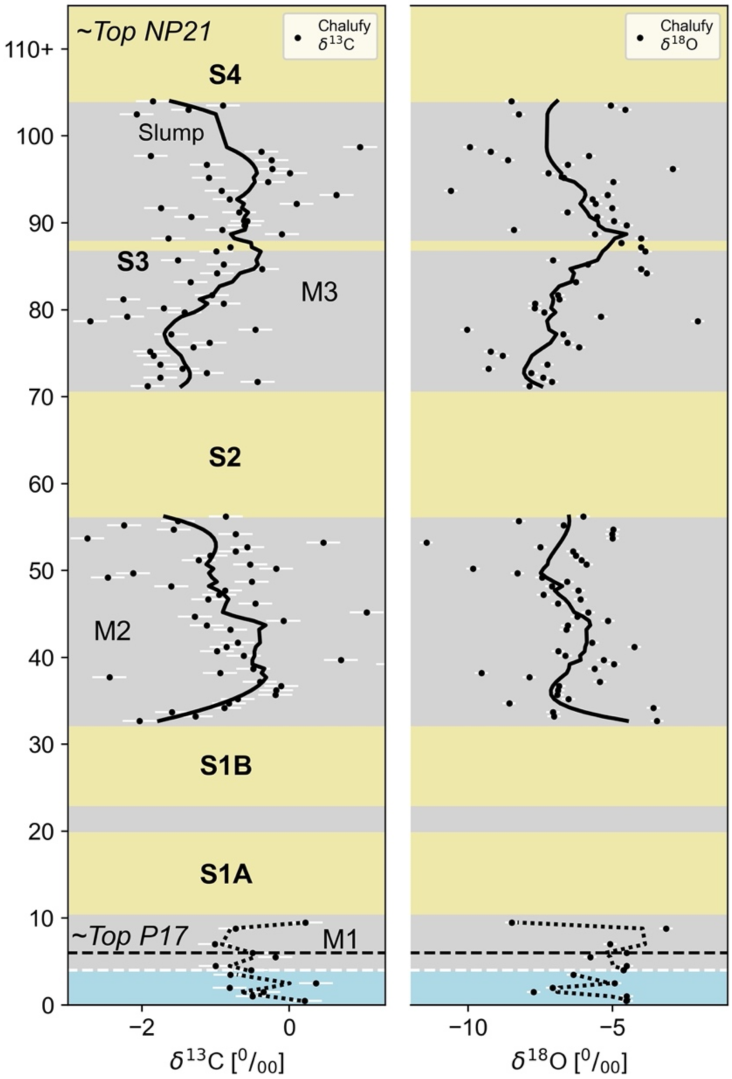
~Top NP21
S4
Slump
S3
M3
S2
M2
S1B
S1A
~Top P17
M1
Chalufy
δ13C
Chalufy
δ18O
110+
100
90
80
70
60
50
40
30
20
10
0
−2
0
−10
−5
δ13C [0/00]
δ18O [0/00]

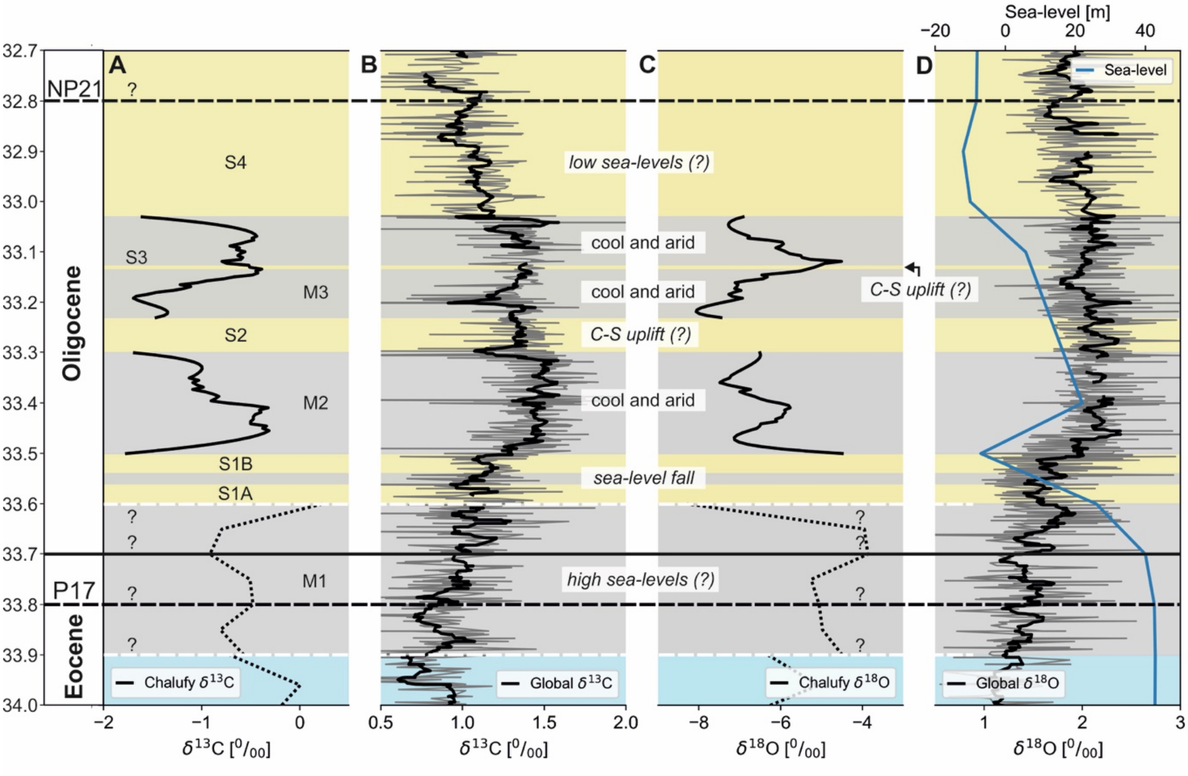

A
B
C
D
NP21
P17
Oligocene
Eocene
S4
S3
M3
S2
M2
S1B
S1A
M1
low sea-levels (?)
cool and arid
cool and arid
C-S uplift (?)
cool and arid
sea-level fall
high sea-levels (?)
C-S uplift (?)
Sea-level [m]
Sea-level
Chalufy δ13C
Global δ13C
Chalufy δ18O
Global δ18O
δ13C [0/00]
δ13C [0/00]
δ18O [0/00]
δ18O [0/00]

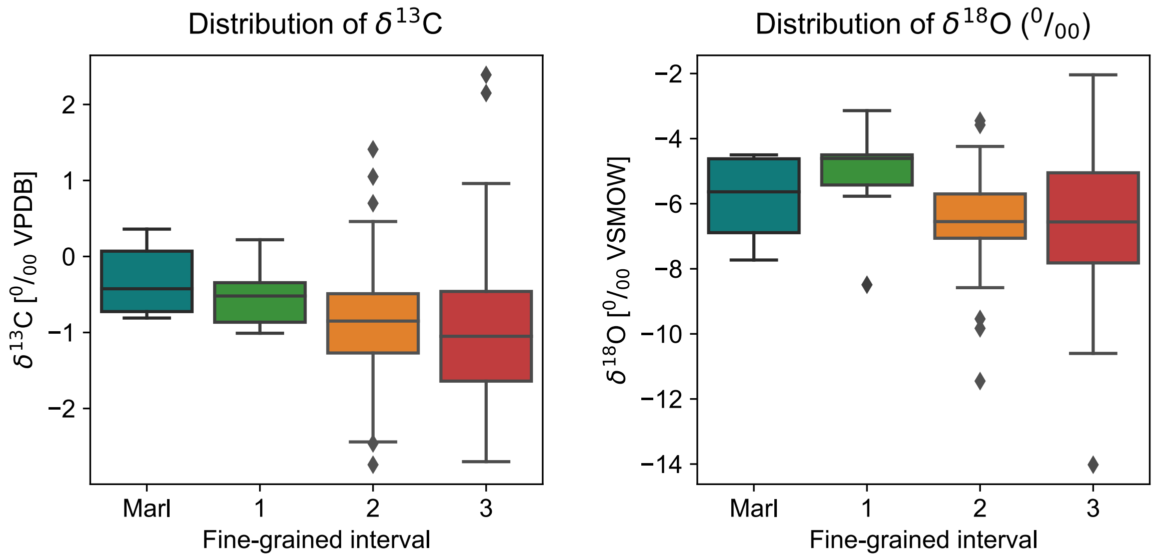
Distribution of δ13C
δ13C [0/00 VPDB]
2
1
0
−1
−2
Marl
1
2
3
Fine-grained interval
Distribution of δ18O (0/00)
δ18O [0/00 VSMOW]
−2
−4
−6
−8
−10
−12
−14
Marl
1
2
3
Fine-grained interval

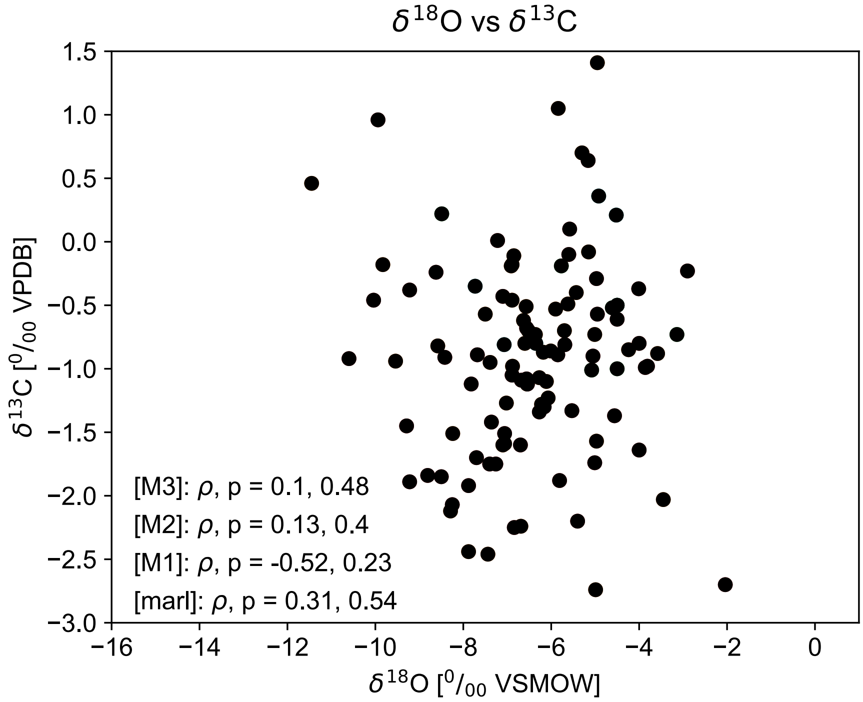

δ^{18}O vs δ^{13}C
δ^{13}C [$^0/_{00}$ VPDB]
δ^{18}O [$^0/_{00}$ VSMOW]
[M3]: ρ, p = 0.1, 0.48
[M2]: ρ, p = 0.13, 0.4
[M1]: ρ, p = -0.52, 0.23
[marl]: ρ, p = 0.31, 0.54

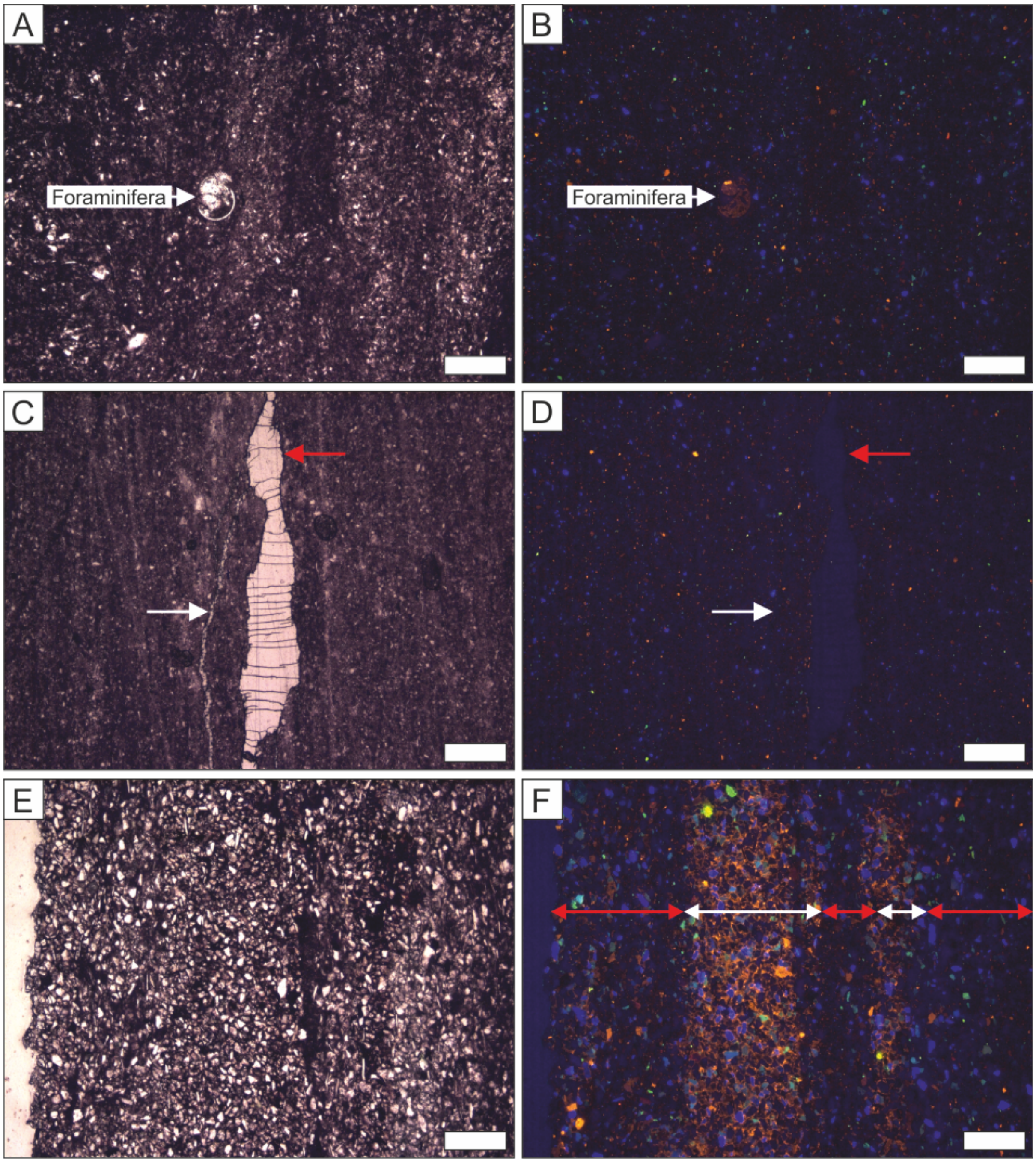
A
Foraminifera
B
Foraminifera
C
D
E
F

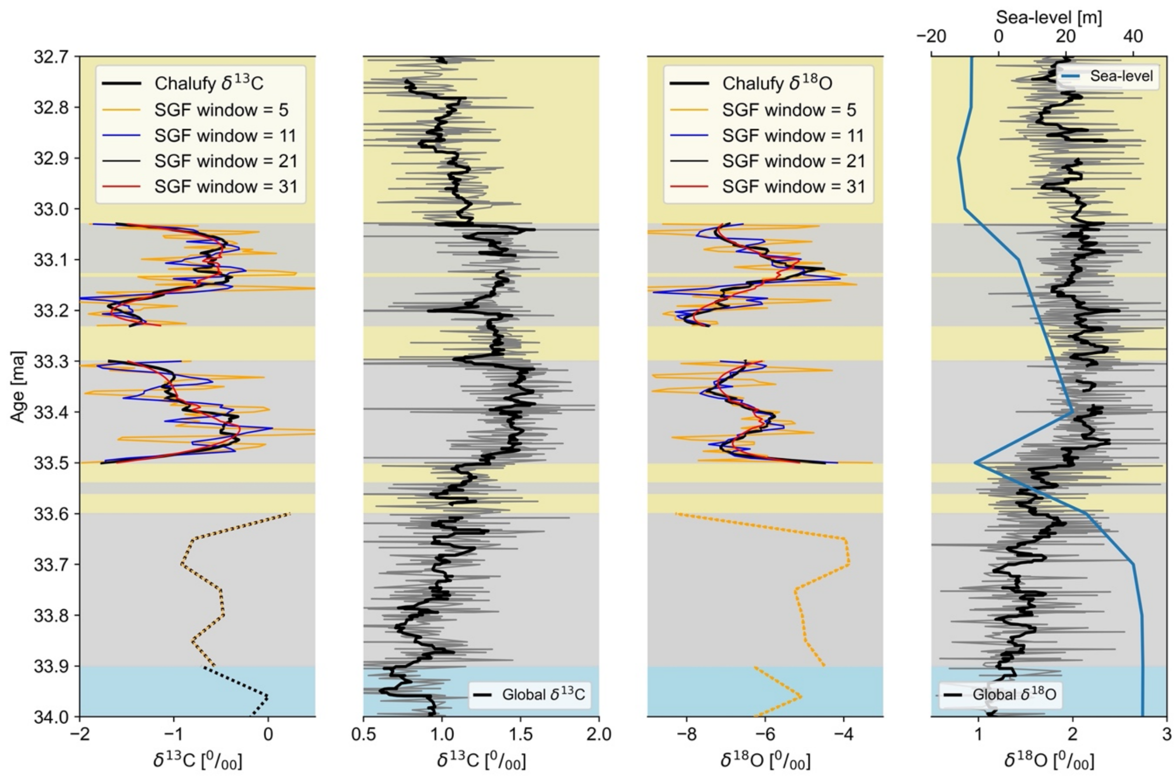

Chalufy δ^{13}C
SGF window = 5
SGF window = 11
SGF window = 21
SGF window = 31
Age [ma]
δ^{13}C [$^0/_{00}$]
Global δ^{13}C
Chalufy δ^{18}O
δ^{18}O [$^0/_{00}$]
Sea-level [m]
Sea-level
Global δ^{18}O